Letter

Few-cycle vortices from superradiant nonlinear Thomson scattering by a relativistic chirped mirror

B. H. Schaap,[1,*] P. W. Smorenburg,[2] and O. J. Luiten[1]

[1]*Department of Applied Physics, Eindhoven University of Technology, P.O. Box 513, 5600 MB Eindhoven, The Netherlands*

[2]*ASML Netherlands B.V., P.O. Box 324, 5500 AH Veldhoven, The Netherlands*

(Received 21 December 2022; accepted 14 July 2023; published 12 September 2023)

We propose a scheme to generate few-cycle vortices based on nonlinear Thomson scattering by microbunched electrons from a circularly polarized laser pulse with chirped frequency. At sufficiently high intensities, the generation of harmonics that carry orbital angular momentum occurs. At the same time, the electrons collectively act as a relativistic chirped mirror, which superradiantly reflects a chosen harmonic into a single localized beat. Calculations show that a few-cycle soft x-ray vortex with gigawatt peak power can be generated if this scheme is applied to a pC electron bunch with a few MeV kinetic beam energy.

DOI: 10.1103/PhysRevResearch.5.L032034

Electromagnetic fields with an azimuthal phase dependence $\exp(i\ell\phi)$ along the direction of propagation carry orbital angular momentum (OAM) with quantum number ℓ [1]. In the optical regime, these so-called vortex beams are an indispensable tool for fundamental research [2,3] and applications in optical manipulation, communication, imaging, and quantum optics [4–10]. Extreme-ultraviolet and x-ray vortices, owing to a significantly lower diffraction limit, extend these applications to the atomic and molecular length scale, and allow for sitespecific photoexcitation and ionization, with important applications in spectroscopy and microscopy [11–13]. Furthermore, due to the short wave cycle in the extreme-ultraviolet and x-ray regime, pulses of attosecond duration can potentially be generated, corresponding to the timescale of electronic motion in atoms and molecules [14].

Conventionally, vortex beams are generated by inserting an optical element, such as a spiral phase plate, into the beam path [15,16]. However, for intense short-wavelength radiation, the damage threshold and fabrication challenges of these elements limit the use of this method. To overcome this, *in situ* generation of vortex beams is favored. High harmonics from laser-atom interaction allows for generation of bursts of attosecond vortices in a compact setup [17–19]. The scaling of high harmonic efficiency, however, limits application in the high photon energy regime [20,21]. In contrast, relativistic electrons in an undulator can be made to emit short-wavelength vortex beams with abundant intensity [22–24]. Yet, this approach comes at the expense of a long pulse length (>10 fs) and requires the use of large scale, costly facilities with limited beam time.

Alternatively, nonlinear Thomson scattering by electrons from an intense laser pulse allows for *in situ* creation of vortices with favorable scaling toward the x- and γ-ray regime [25]. In nonlinear Thomson scattering, a relativistic electron oscillates strongly due to coupling with the electromagnetic field of a laser pulse with a strength parameter $a_0 = eE_0/(m_e c\omega_0) \sim 1$ (with e elementary charge, E_0 the electric field strength, ω_0 the central frequency, m_e the electron mass, and c the speed of light). Head-on collision of the electron with an intense laser pulse results in the emission of harmonics centered at upconverted frequency [26]:

$$\omega_n = \frac{n\omega_0}{1-\beta_1(1+\cos\theta)}, \tag{1}$$

where n is an integer, θ is the emission angle with respect to the electron propagation axis, and $\beta_1 = \{1-(1+a_0^2/2)/[(1+\beta)^2\gamma^2]\}/2$ with $c\beta$ the initial axial velocity and $\gamma = (1-\beta^2)^{-1/2}$ the Lorentz factor. Moreover, the short wavelength of the laser pulse allows for significantly more compact accelerator setups than undulator sources. However, the shortest pulse length is limited by the convolution of the electron bunch and laser pulse length, which typically is on the order of ten to hundreds of femtoseconds, much longer than the electronic time scales.

In this Letter, we propose an approach to generate attosecond vortices via superradiant nonlinear Thomson scattering by colliding an intense circularly polarized laser pulse with a chirped frequency on a relativistic chirped electron mirror such as illustrated in Fig 1. This mirror is an electron bunch with a varying density modulation frequency such that the superposed radiation pulses emitted by each electron form a localized beat, strongly compressing the single electron radiation fields [27]. Here, using the framework of classical electrodynamics, we demonstrate in two steps that this method is applicable in the nonlinear Thomson regime. First, we show that chirped vortices are generated from a chirped laser pulse, which are suitable for compression by a chirped electron mirror. Then, taking into account superradiance by the mirror, we find the conditions under which few-cycle vortices are generated and show that for these parameters multi-GW few-cycle extreme ultraviolet pulses are attainable.

*b.h.schaap@tue.nl

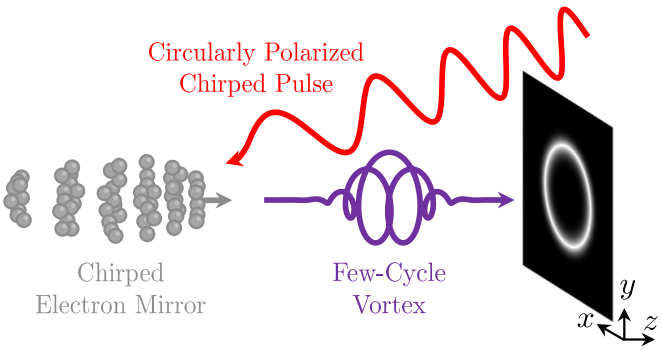

FIG. 1. Schematic of few-cycle vortex generation by reflecting a chirped circularly polarized laser pulse with a relativistic chirped electron mirror.

The spectral electric field at far-field distance r radiated from an arbitrary current density distribution $\mathbf{J}$ is given by [28]

$$\mathbf{E}(\mathbf{r},\omega)=\frac{i\omega e^{i\omega r/c}}{4\pi\epsilon_0 cr}\mathbf{n}\times\mathbf{n}\times\int\mathbf{J}(\mathbf{x},t)e^{i\omega(t-\mathbf{n}\cdot\mathbf{x}/c)}dt\mathbf{dx}, \quad (2)$$

with ω the angular frequency of the radiation, ϵ_0 the vacuum permittivity, and $\mathbf{n}$ the propagation direction of the emitted radiation. From the general expression, Eq. (2), we derive more practical equations for a relativistic chirped mirror that reflects a chirped laser pulse of pulse length T (full width) described by vector potential $\mathbf{A}=m_e c a_0/(\sqrt{2}e)(\cos\Phi\mathbf{e}_x+\sin\Phi\mathbf{e}_y)$, with $\Phi=\omega_0\tau+\alpha\tau^2+\varphi_i$ the laser phase with Galilean time $\tau=t+z/c$, α the chirp rate, and φ_i phase at the center of the pulse where $\tau=0$.

The electric current of the mirror consisting of N electrons is given by $\mathbf{J}=-\sum_{j=1}^{N}e\mathbf{v}_j\delta^{(3)}(\mathbf{x}-\mathbf{x}_j)$ with $\delta^{(3)}(x)$ the three dimensional Dirac delta function, $\mathbf{x}_j$ the electron trajectory, and $\mathbf{v}_j$ the velocity. We find by solving the Lorentz force equation that an electron during interaction has a constant axial velocity and makes helical transverse oscillations that are described by (see the Appendix)

$$\mathbf{x}_j=\mathbf{x}_{0,j}+\frac{r_0}{1+\alpha\tau/\omega_0}(\sin\Phi\,\mathbf{e}_x-\cos\Phi\,\mathbf{e}_y)+c\beta_1\tau\,\mathbf{e}_z, \quad (3)$$

with $x_{0,j}$ the initial position and $r_0=a_0/[\sqrt{2}k_0\gamma(1+\beta)]$. Here, the term between brackets describes the transverse spiral motion induced by the laser pulse. The spiral radius is proportional to the optical quasiperiod that changes linearly along the laser pulse axis. At the center of the interaction when $\tau=0$, the radius is equal to r_0. The last term in Eq. (3) describes the uniform axial motion during interaction, with a velocity that is lower than the axial velocity prior to interaction as a result of the relativistic transverse motion. Since the particle velocity as function of time t is given by $\mathbf{v}_j=(d\mathbf{x}_j/d\tau)d\tau/dt$, the axial velocity is given by $v_z=c\beta_1/(1-\beta_1)$.

Substituting the electron trajectory, given by Eq. (3), and the corresponding velocity into the general expression for the field, given by Eq. (2), we find that the field emitted by a single electron can be decomposed in harmonics such that $\mathbf{E}_j=\sum_{n=1}^{\infty}\mathbf{E}_{n,j}$. The field of the nth harmonic is given by (see the Appendix)

$$\mathbf{E}_{n,j}(r,\theta,\phi,\omega)=\frac{ie\omega Te^{i\omega r/c-\varphi_{0,j}}}{4\pi\epsilon_0 cr}F_n(\omega,\theta)\times[JJ_n^{+}(\theta)e^{i(n-1)\phi}\mathbf{e}_{+}+JJ_n^{-}(\theta)e^{i(n+1)\phi}\mathbf{e}_{-}], \quad (4)$$

with $\varphi_{0,j}=n\varphi_i+\omega(\mathbf{n}\cdot\mathbf{x}_{0,j}+z_{0,j})/c$ a constant phase offset, F_n the linewidth function, $JJ_n^{\pm}=[k_0r_0J_{n\pm1}(\zeta_n)-(1-\beta_1)\sin\theta J_n(\zeta_n)]/\sqrt{2}$, with $\zeta_n=\omega_n r_0\sin\theta/c$, the emission amplitudes and $\mathbf{e}_{\pm}=(\mathbf{e}_x\pm i\mathbf{e}_y)/\sqrt{2}$ complex unit vectors describing circular polarization with positive and negative helicity, respectively. The emitted electric field is thus an elliptically polarized vortex field that can be decomposed in components having positive helicity with orbital angular momentum of $\ell=n-1$ and negative helicity with $\ell=n+1$ orbital angular momentum. The respective weight of the polarization states is determined by the emission amplitudes. In Eq. (4) we neglected the longitudinal field component, which in all practical cases is much smaller than the transverse components.

The spectral response of the single electron emission is expressed by the linewidth function

$$F_n=\sqrt{\frac{\pi}{2n\alpha T^2}}[Z(u_n^{+})-Z(u_n^{-})]e^{i\Gamma_n(\omega-\omega_n)^2}, \quad (5)$$

where $Z(x)=\int_0^x\exp[-i\pi y^2/2]dy$ is a complex Fresnel integral, $u_n^{\pm}=(\omega-\omega_n)\sqrt{\Gamma_n/\pi}\pm\sqrt{n\alpha T^2/(4\pi)}$, and $\Gamma_n=[1-\beta_1(1+\cos\theta)]^2/(n\alpha)$ is the group delay dispersion of the emitted radiation, which quantifies the spectral delay with respect to the center of the pulse. For the quasimonochromatic case $\alpha=0$, the linewidth function is $F_n\simeq\mathrm{sinc}[T_1(\omega-\omega_n)/2]$, where $\mathrm{sinc}(x)=\sin(x)/x$ is the cardinal sine and $T_1=T[1-\beta_1(1+\cos\theta)]$ is the single electron radiation (full width) pulse length, and Eq. (4) reduces to the spectral field for nonlinear Thomson scattering from an unchirped laser pulse [25,26]. On the other hand, for strongly chirped laser pulses, i.e., when the frequency chirp αT is much larger than the transform limited bandwidth T^{-1} of an unchirped laser of the same length, the complex Fresnel integrals in Eq. (5) can be approximated by a rectangular distribution function $Z(u_n^{+})-Z(u_n^{+})\simeq\Pi[(\omega-\omega_n)/\Delta\omega_n]$ with $\Delta\omega_n=(n\alpha T)/[1-\beta_1(1+\cos\theta)]$ the spectral bandwidth. In this regime, in contrast to the unchirped case, the amplitude decreases and the bandwidth of the emitted pulse increases with n. The latter is an important feature for the generation of monocycle vortices, which requires a large bandwidth.

Figure 2(a) shows the spectral angular energy distribution $d^2W_j/(d\Omega d\omega)=\epsilon_0cr^2\sum_{n=1}^{\infty}|\mathbf{E}_{n,j}(\omega)|^2$ in the $\phi=0$ plane of a single electron with 3.1 MeV kinetic energy reflecting a head-on 1 ps chirped laser pulse with strength $a_0=1$, central wavelength of $\lambda_0=1$ μm, and chirp rate $\alpha=0.3$ THz/fs. The central wavelength of the fundamental emitted on-axis is 7.5 nm in this scattering geometry. Due to the symmetry of the electron trajectory the energy distribution is independent of ϕ. The fundamental is most intense on-axis and is contained within a half angle of approximately $1/\gamma$. The higher harmonics have an annular radiation pattern with no emission on-axis, which is customary for vortex beams. The

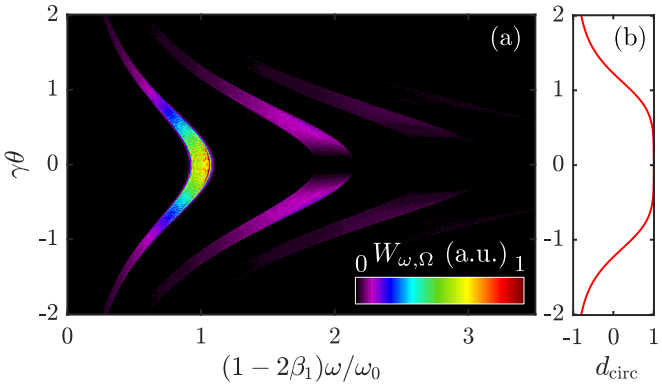

FIG. 2. (a) Spectral angular distribution of single electron nonlinear Thomson scattering from a chirped laser pulse. (b) Degree of circular polarization.

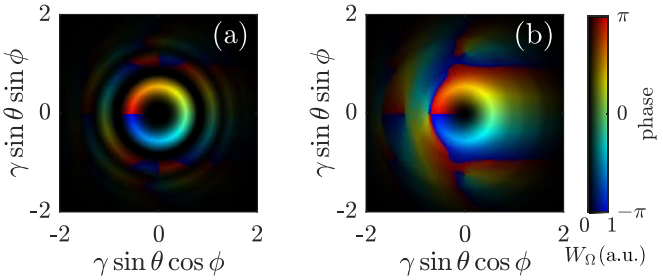

FIG. 3. Superradiant intensity and phase pattern for $\alpha =$ 0.3 THz/fs (a) and 0.75 THz/fs (b). The color corresponds to the phase the pixel corresponds to the radiation intensity.

angle of largest intensity increases with harmonic and, under the assumptions that $a_0 \leqslant 1$ and $\gamma \gg 1$, is found approximately at angle $\gamma\theta_{\rm max} = \sqrt{1+a_0^2/2}\sqrt{(n-1)/(n+3)}$. The figure also confirms that the bandwidth of the higher harmonics increases. At harmonic order $n_{\rm max} = \omega_0/(\alpha T) - 1/2$, the spectral contributions will start to significantly overlap making compression, discussed later on, impractical.

The degree of circular polarization $d_{\rm circ} = (|E_+|^2 - |E_-|^2)/(E_+|^2 + |E_-|^2)$, with $E_\pm$ the electric field amplitude of the positive and negative helicity component, is plotted in Fig. 2(b). The degree of polarization is the same for all harmonics. Near the electron propagation axis, the polarization is almost completely circularly polarized with positive helicity. This implies that here the radiation carries orbital angular momentum with quantum number $\ell = n - 1$. Off-axis, the polarization first becomes elliptical, and then, for these parameters, around $\theta = 1/\gamma$, linear ($d_{\rm circ} = 0$) corresponding to a superposition of orbital angular momentum states. Note that especially for lower order harmonics, the intensity has reduced significantly at this point. At even larger angles, the polarization goes from elliptical to fully circular with negative helicity ($d_{\rm circ} = -1$) indicating that the $\ell = n + 1$ state is dominant. These results coincide with the polarization from the unchirped case found in [25,29].

So far, we described the spectral electric field emitted by an individual electron that collides with a chirped laser pulse. Now, we will take the coherent superposition of such fields, also known as superradiance, from electrons in an electron bunch with a chirped density modulation. Superradiance has been proposed to boost the yield of a Thomson scattering source by orders of magnitude [30,31]. Furthermore, superradiant linear Thomson scattering from a chirped electron mirror has been considered to generate attosecond x-ray pulses [27]. Here, we will show that superradiance from a chirped electron mirror in the nonlinear regime leads to fewcycle soft x-ray pulse with orbital angular momentum.

The superradiant field in the spectral domain is given by the multiplication of the single electron spectral angular distribution and the mirror bunching factor, written as $\mathbf{E}_n(\omega) = N\mathbf{E}_{n,j=0}(\omega)b(\omega)$, where $b(\omega) = 1/N\int_{-\infty}^{\infty} n_e(\mathbf{x})\exp[-i\varphi(\mathbf{x})]d\mathbf{x}$ is the mirror bunching factor with $n_e(\mathbf{x})$ the electron density distribution and $\varphi(\mathbf{x}) = \omega(\mathbf{n}\cdot\mathbf{x} + (1-\beta_1)z)/c$ the phase difference between emission from different parts of the mirror separated by $\mathbf{x}$. For the following calculations we will use an infinitely thin, strongly chirped electron mirror with density distribution given by $n_e = N/(v_z T_e)[1 + 2b_1\cos(\omega_e z/v_z + \alpha_e^2 z^2/v_z^2)]$, where T_e is the (full width) mirror length, $b_1 = [0, 0.5]$ the modulation depth, ω_e the central angular modulation frequency, and α_e the chirp rate. Note that other microbunch distributions or higher harmonic bunching can also be considered, however, this does not significantly change any of the relevant physics.

The bunching factor for this density distribution is similar to the linewidth function of the single electron radiation: For strong chirp, the positive nonzero frequency component of the bunching factor is approximately given by $b(\omega) = \sqrt{b_1^2\pi/(2m\alpha_e T_e^2)}\Pi[(\omega-\omega_e')/\Delta\omega_e]\exp[-i\Gamma_e(\omega - \omega_e')]$, with $\Gamma_e = \beta_1^2(1+\cos\theta)^2/(m\alpha_e)$ the group delay dispersion determining the chromatic dispersion of the mirror, $\Delta\omega_e = m\alpha_e T_e/[\beta_1(1+\cos\theta)]$ the bandwidth of the mirror, and central frequency of superradiance given by

$$\omega_e' = \frac{\omega_e}{\beta_1(1+\cos\theta)}. \tag{6}$$

To overlap the superradiant emission of all frequencies within harmonic n in time, the periodic density modulation of the mirror should satisfy the following three conditions. First, the variation in bunching frequency should be large enough to support superradiant reflection of the full laser bandwidth such that $\Delta\omega_e \geqslant \Delta\omega_n$. Second, the central superradiant frequency should be centered around the central emission frequency, leading to a bunching frequency of $\omega_e = n\omega_0\beta_1(1+\cos\theta)/[1-\beta_1(1+\cos\theta)]$. Last, the superradiant reflection of each spectral component should occur in a single beat, which can only hold true if the dispersion of the mirror is equal to the dispersion of the single electron radiation pulse which occurs for a bunching chirp rate given by $\alpha_e = n\alpha\beta_1^2(1+\cos\theta)^2/[1-\beta_1(1+\cos\theta)]^2$. To generate ultrashort vortices, the latter conditions should hold off-axis.

In Figs. 3(a) and 3(b) the angular energy distribution $dW/d\Omega = \epsilon_0 cr^2\sum_{n=1}^{\infty}\int d\omega|\mathbf{E}_n(\omega)|^2$ and the phase of (the part between squared brackets of) the electric field given by Eq. (4) resulting from a $T_e = 9.1$ fs chirped electron mirror with 3.1 MeV kinetic energy, tuned to amplification of the second harmonic at $\gamma\theta_{\rm max} \simeq 0.54$ from a 1 ps laser pulse of

$a_0 = 1$ with central wavelength of $\lambda_0 = 1$ μm is shown for two cases. First, the same chirping parameters are used as in Fig. 2. In Fig. 3(a) the intensity pattern consists of spatially separated rings of varying amplitude. The brightest ring, found at the maximum scattering angle, is the amplified second harmonic with a central wavelength of 4.5 nm close to the K-absorption edge of carbon. Each ring farther out corresponds to a higher order harmonic, which, due to the relativistic Doppler shift, have a nonzero contribution in the superradiant bandwidth. Second, the intensity pattern for a laser pulse with the largest chirp $\alpha = 0.75$ THz/fs that still allows for compression of the second harmonic is shown in Fig. 3(b). The separate harmonic rings join to form a single broadband annular radiation pulse. The angular spread in this case has greatly increased resulting from the larger bandwidth induced by the laser pulse. Note that the intensity distribution is independent of dispersion matching.

The phase corresponding to previous cases is plotted in the same figure. For the first case the phase makes one rotation closest to the axis, corresponding to orbital angular momentum of $\ell = 1$, for which the system is optimized. Going farther off-axis one finds higher levels of orbital angular momentum related to the increasing harmonic order. The harmonic orders remains quite well separated until very large angles. In contrast, for the large bandwidth case, harmonics larger than the second already overlap leading to a complex distribution of phase indicating ill-defined orbital angular momentum. However, this undesired part of the beam can easily be removed with a spatial filter.

If the dispersion is matched correctly along a chosen scattering angle θ_V, a time-compressed vortex beam is generated. The electric field in the temporal domain for this case can be calculated analytically by taking the inverse Fourier transform of the spectral field, which is given by

$$\begin{aligned}\mathbf{E}_{\mathrm{V}}(r,\theta_V,\phi,t) &= i\frac{Qb_1}{8\epsilon_0 cr}\frac{T}{T_e\beta_1(1+\cos\theta_V)}JJ_n^+\frac{\partial}{\partial(t-r/c)} \\ &\times e^{-i\omega_n(t-r/c)+i(n-1)\phi+in\varphi_i}\mathrm{sinc}\left[\pi\frac{t-r/c}{T_{\mathrm{V}}}\right]\mathbf{e}_+, \quad (7)\end{aligned}$$

where we assumed that the compression occurs close to the angle at which the single electron intensity is largest, so we can neglect the components with negative helicity. The pulse length—taken to be the first intensity node of the pulse—is given by

$$T_{\mathrm{V}} = 2\pi\frac{1-\beta_1(1+\cos\theta_V)}{n\alpha T}, \quad (8)$$

which is equal to Fourier-limited pulse length allowed by the bandwidth of the corresponding harmonic emitted by a single electron, and $Q = -eN$ is the total charge of the mirror. The compressed pulse length is fully determined by the nonlinear Doppler shift, the harmonic number n, and the laser bandwidth. Thus, the shortest vortex attainable is limited by bandwidth overlap. Using the condition for $n_{\max}$ and Eqs. (1) and (8), we find that the smallest number of cycles of a vortex with $\ell = n_{\max} - 1$ using the method described in this paper is given by $N_{\min} = \omega_n T_V/(2\pi) = n_{\max} + 1/2$. In Fig. 4 the time-dependent electric field is plotted for the same parameters as

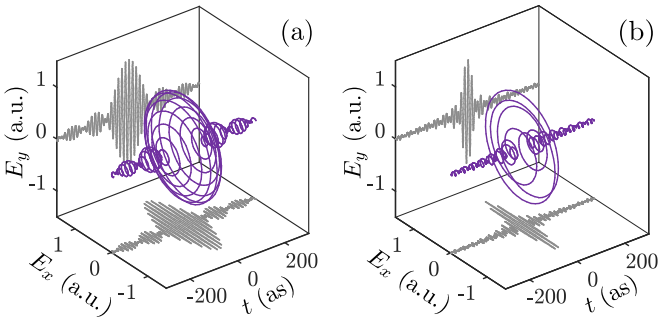

FIG. 4. Time-dependent electric field along matching angle at $\phi = 0$ for $\alpha = 0.3$ THz/fs (a) and 0.75 THz/fs (b).

the previous cases. For the first case (a) the pulse length is given by $T_{\mathrm{V}} = 94$ as, and the second case $T_{\mathrm{V}} = 37$ as (b) corresponding to 6.3 and 2.5 cycles, respectively. The latter has yet to be demonstrated in any kind of source even for pulse carrying no orbital angular momentum. The uncompressed single electron field has a pulse length of 9 fs, a few orders of magnitude longer.

Well-compressed radiation is limited to the angular range where the delay induced by the group delay dispersion mismatching $(\Gamma_n - \Gamma_e)\Delta\omega_n$ becomes on the order of the compressed pulse length T_{V}. Assuming the mirror dispersion does not change considerably, we find that the angular range of compression is about $\Delta\theta_c = \pi(1 + a_0^2/2)/(\gamma^2\theta_V n\alpha T^2)$, which for strong compression is much smaller than the angular spread of the intensity.

One may raise the question if strongly compressed vortices have abundant power. Therefore, we calculate the pulse energy and peak power for this case. The pulse energy of the compressed pulse is given by $W = \int_0^{2\pi}\int_{\theta_V-\Delta\theta_V/2}^{\theta_V+\Delta\theta_V/2} d\omega d\Omega\epsilon_0 cr^2|\mathbf{E}(\omega)|^2 \simeq Q^2 b_1^2 JJ_n^{+2}\omega_n^4 T_{\mathrm{V}}\theta_{\mathrm{V}}$ $\Delta\theta_c/(16\epsilon_0 c\omega_0^2)$ with $d\Omega = \sin\theta d\theta d\phi$ is the differential solid angle and JJ_n^+ is evaluated at θ_V. The vortex pulse energy using the same parameters with a bunch charge $Q = 3$ pC, and density modulation of $b_1 = 0.5$ is $W = 0.88$ μJ for the first case and $W = 0.14$ μJ for the few-cycle case. The latter contains less energy due to the smaller angular spread of compression. The difference in the resulting peak power $P = W/T_{\mathrm{V}}$, however, is smaller: 9.3 GW and 3.7 GW, respectively. Electromagnetic pulses at a frequency near the water window with this amount of pulse energy and peak power are only available in free electron laser sources [32], without carrying orbital angular momentum.

Several physical considerations are in place for realization of this scheme. First, compression is impacted when the delay of the mirror changes significantly with respect to the single electron radiation. The compression is not affected as long as the electron beam energy spread $\Delta\gamma$, the electron beam angular spread $\Delta\theta_e$ or the (transverse and longitudinal) laser strength variation variation Δa_0 satisfies the condition $(4\Delta\gamma^2/\gamma^2 + \gamma^4\Delta\theta_e^4 + \Delta a_0^4/4)^{1/2} \leqslant \gamma^2\Delta\theta_c^2$. For the extreme case of few-cycle vortex generation, the relative energy spread, for example, should be lower than 10^{-5}. For the other case, the condition for the energy spread is relaxed by an order of magnitude.

Second, the transverse mirror width might significantly inhibit the superradiance at the scattering angles where the OAM is present, due to destructive interference of the emitted coherent light fields [31]. The superradiance along the compression angle θ_V is not significantly affected as long as the mirror width $\sigma_\perp$ satisfies the condition $\sigma_\perp \leqslant c/(\omega_n \theta_V)$. For both the previous cases, the waist should be smaller than about 10 nm, which is difficult to attain at high charge due to space charge forces or without allowing significant detrimental angular spread. This can be overcome by going to higher electron beam energy or by tailoring the density distribution such that an off-axis angle is favored by superradiance.

Last, it is challenging to generate the intricate density modulation required for compression. Methods have been have proposed [33] and demonstrated [34] at high energy. At the relevant beam energy, an energy modulation that converts into a density modulation can be attained via the ponderomotive force resulting from the beat wave formed two laser pulses [35,36], which can be generalized to chirped modulation by using a few-cycle and a chirped laser pulse. Another method that potentially allows for the generation of the intricate density modulation is the use of dielectric laser accelerators [37].

In summary, we propose a method to generate few-cycle vortex beams from nonlinear scattering by a chirped electron mirror that acts simultaneously, as a frequency shifter, mode converter, and compressor. We find that the higher order harmonics are suitable for compression to few cycles, limited by spectral overlap with neighboring harmonics. Calculations show that soft x-ray vortices with gigawatt peak power are attainable using this method using bunch charge of several pC. These findings can have great impact for the development of compact powerful soft x-ray sources. While we propose the generation of soft x-ray vortices, the theory is universally scalable over the electromagnetic spectrum.

This research was funded by the Ministry of Economic Affairs in the Netherlands through a TKI grant.

APPENDIX: DERIVATION OF CHIRPED VORTEX FOUR POTENTIAL

We describe the interaction between an electron and a laser pulse in the framework of covariant electrodynamics, using the metric $g^{\mu\nu} = \mathrm{diag}(1, -1, -1, -1)$. In this classical description we neglect electron recoil, restricting the initial central laser frequency ω_0 to fulfill the condition $\gamma \hbar \omega_0/(m_e c^2) \ll 1$, where γ_0 is the Lorentz factor of the electron prior to interaction, $\hbar$ the reduced Planck's constant, c the speed of light, and m_e the electron mass.

We calculate the far-field vortex four potential in the time-spectral domain from the solution to the inhomogeneous wave equation in the Lorentz gauge, which in normalized form can be written as

$$A^\mu_{\mathrm{rad}}(\mathbf{r}, \omega) = \mathrm{O}(r, \omega) \sum_{j=1}^{N_e} \int u^\mu_j e^{i k^\nu x_{j\nu}} d\tau \qquad \text{(A1)}$$

with $\mathrm{O}(r, \omega) = (r_e/r) \exp(i\omega r/c)$ a quasiinvariant describing the spatial component of a spherical wave at position r far from the center of interaction, ω the angular frequency, and r_e the classical electron radius. The summation over N_e electrons describes the spectral four current of the mirror, where u^μ_j is the four velocity of the jth electron, x^μ_j the four position, and $k^\mu = \omega/c(1, \mathbf{e}_r)$ the four wave vector of the radiation field. The present section is organized as follows: First, the trajectories of a single electron in a CPC laser pulse are calculated. Then, an expression for the single electron four potential is derived to show azimuthal phase dependence.

1. Electron dynamics in chirped laser pulse

The trajectories of an electron in a laser pulse can be calculated by integrating the Lorentz force equation $\partial_\tau u^\mu = u_\nu(\partial^\nu A^\mu - \partial^\mu A^\nu)$. For any four-potential A^μ that only depends on laser phase variable $\varphi = k^\nu_0 x_\nu$, with k^μ_0 the four wave vector of the laser pulse, the solution to the Lorentz force is given exactly by

$$u^\mu = u^\mu_0 + A^\mu - \frac{1}{\kappa}\left[\frac{1}{2}A^\nu A_\nu + u^\nu_0 A_\nu\right] k^\mu_0, \qquad \text{(A2)}$$

where u^μ_0 is the initial four velocity normalized to the speed of light, and $\kappa = \partial_\tau \varphi = k^\nu_0 u_{0\nu}$ is the light cone variable, which describes the central wave number of the laser in the instantaneous rest frame of the electron prior to interaction. The terms scaling linearly in A^μ describe the coupling of the electron to the electric and magnetic field. The quadratic term describes the momentum resulting from the ponderomotive force.

In earlier work, expressions for the electron trajectories induced by a counterpropagating intense circularly polarized laser pulse have been found analytically [25]. Here, we extend those calculations to a circularly polarized laser pulse at linearly chirped angular frequency $\Omega = \omega_0(1 + \alpha\varphi)$, where α is the normalized chirp rate. The normalized four potential of the chirped laser pulse is given by

$$A^\mu_{\mathrm{CCP}} = a_0 \exp\left[-i\left(\varphi + \frac{\alpha}{2}\varphi^2\right)\right] \Pi\left(\frac{\varphi}{\Delta\varphi}\right) \epsilon^\mu, \qquad \text{(A3)}$$

where a_0 is the laser strength parameter, the function $\Pi(\varphi/\Delta\varphi) = \Theta(\varphi + \Delta\varphi/2) - \Theta(\varphi - \Delta\varphi/2)$, with $\Theta(x)$ the Heaviside step function, describes the rectangular envelope of the laser pulse of length $\Delta\varphi$, and $\epsilon^\mu = (0, 1, i, 0)/\sqrt{2}$ is the polarization four vector. For circular polarization, the ponderomotive term in Eq. (A2) is a constant $A^\nu A_\nu = -a_0^2/2$, reducing the longitudinal momentum of the time-averaged four velocity $\bar{u}^\mu = u^\mu_0 + a_0^2/(4\kappa)k^\mu_0$ during interaction. Physically, this results from the ponderomotive force from the front of the laser pulse.

The electron trajectories can be calculated as function of optical phase φ by plugging Eq. (A3) into (A2) using the relation $\partial_\tau x = \kappa \partial_\varphi x$. For a counterpropagating electron $u^\nu_0 A_\nu = 0$, the four position is written as

$$x^\mu = x^\mu_0 + \frac{1}{\kappa}\left[\bar{u}^\mu \varphi + \; i A^\mu_{\mathrm{CPC}} \frac{\omega_0}{\Omega}\left(1 + \sum_{n=1}^{\infty} \chi_n\right)\right] \qquad \text{(A4)}$$

with $\chi_n = (i\alpha\omega_0^2\Omega^{-2})^n(2n-1)!!$ terms resulting from integrating by parts iteratively. Here, x^μ_0 is the initial four position of the electron in respect to the laser phase. The second term describes the uniform motion by the average velocity of the electron in the laser field. The last accounts for the quiver motion with an amplitude that is proportional to the quasiperiod

$T = 2\pi/\Omega$. In the following we assume that there is a notion of a quasiperiod, such that the condition $|\chi_n| \ll 1$ holds and the higher order correction terms can be neglected. It is important to note here that x^μ depends on φ and vice versa. Hence, it is a recursive relation, which we must readdress for a correct description of superradiance by the mirror later on.

2. Single electron four potential

We can now calculate the time-spectral radiation four potential (A1). By filling in the real part of Eq. (A4), the phase of the integrand can be written in the form

$$k^\nu x_{j\nu} = \frac{k^\nu \bar{u}_\nu}{\kappa}\varphi - \zeta \sin\left(\varphi + \frac{\alpha}{2}\varphi^2 - \phi\right) \tag{A5}$$

with $\zeta = a_0\omega\sin\theta/(\sqrt{2}c\kappa(1+\alpha\varphi))$, θ the scattering angle, and ϕ the azimuthal angle. The sinusoidal part of Eq. (A5) in the exponent can be written as the sum of Bessel functions J_n of integer n using the Jacobi-Anger expansion $\exp(-iz\sin x) = \sum_{n=-\infty}^{\infty} J_n(z)\exp(-inx)$. After sorting the indices, the integrand of Eq. (A1) can be written as

$$\sum_{n=-\infty}^{\infty} a_n^\mu \exp\left[i(k^\nu\bar{u}_\nu/\kappa - n)\varphi - in\frac{\alpha}{2}\varphi^2\right]$$

with vector amplitude

$$a_n^\mu(\zeta) = J_n(\zeta)e^{in\phi}\bar{u}^\mu + \tfrac{1}{2}a_0 J_{n-1}(\zeta)e^{i(n-1)\phi}\epsilon^\mu + \tfrac{1}{2}a_0 J_{n+1}(\zeta)e^{i(n+1)\phi}\epsilon^{*\mu},$$

which already clearly shows azimuthal phase dependencies. In contrast to the complex exponent, the vector amplitude is slowly varying in φ. The largest part of the integral will therefore come from stationary phase $\varphi_s = (k^\nu\bar{u}_\nu/(n\kappa) - 1)/\alpha$. Expanding a^μ around φ_s to zeroth order changes the argument of the Bessel functions to $\zeta_n = na_0 k\sin\theta/(\sqrt{2}k^\nu\bar{u}_\nu)$, resulting in

$$A^{(1)\mu}_{\mathrm{rad,n}}(\mathbf{r},\omega) = \frac{\Delta\varphi}{\kappa}\mathrm{O}(r,\omega)a_n^\mu(\zeta_n)F_n, \tag{A6}$$

where F_n is the linewidth function that describes the spectral response of the single lecron radiation to the chirped laser pulse, given by

$$\begin{aligned} F_n &= \frac{1}{\Delta\varphi}\int_{-\Delta\varphi/2}^{\Delta\varphi/2}\exp\left[i(k^\nu\bar{u}_\nu/\kappa - n)\varphi - in\frac{\alpha}{2}\varphi^2\right]d\varphi, \\ &= \sqrt{\frac{\pi}{2n\alpha\Delta\varphi^2}}e^{i(\omega/\omega_n-1)^2 n/\alpha}[Z(u_n^+) - Z(u_n^-)], \end{aligned} \tag{A7}$$

where $Z(x) = \int_0^x \exp[-i\pi y^2/2]dy$ is a complex Fresnel integral and $u_n^\pm = (\omega/\omega_n - 1)/\sqrt{n\alpha\pi} \pm \sqrt{n\alpha/(4\pi)}\Delta\varphi$. For unchirped laser pulses $\alpha = 0$, the linewidth function reduces to the conventional form $F_n = \mathrm{sinc}[n\Delta\varphi(\omega/\omega_n - 1)/2]$, where $\mathrm{sinc}(x) = \sin(x)/x$ is the cardinal sine. For strongly chirped laser pulse, i.e., when the relative frequency chirp $\alpha\Delta\varphi$ is much larger than the transform limited relative bandwidth $\Delta\varphi^{-1}$, the complex Fresnel integrals in Eq. (A7) can be approximated by a rectrangular function $\Pi[(\omega/\omega_n - 1)/(\alpha\Delta\varphi)]$.

3. Single electron electric vortex field

In the far field, the differential operator $d^{\mu\nu} = i\omega g^{\mu\nu} - ick^\mu u^\nu_{\mathrm{obs}}$, where u^μ_{obs} is an observer four velocity, can be used to calculate the spectral four field $E^\mu_{\mathrm{rad}} = d^\mu_\nu A^\nu_{\mathrm{rad}}$. In the laboratory frame, where $u^\mu_{\mathrm{obs}} = (1,\mathbf{0})$, application of this operator to the general expression for the radiation four potential, given by Eq. (A1), gives a temporal component equal to zero and the spatial part equal to Eq. (2) in the manuscript. Applying the differential operator to the (spatial part of the) single electron vortex potential results in the following (normalized) spectral electric field

$$\begin{aligned} \mathbf{E}^{(1)}_{\mathrm{rad,n}}(r,\theta,\phi,\omega) &= i\omega\frac{\Delta\varphi}{\kappa}\mathrm{O}F_n\left[J_n(\zeta_n)e^{in\phi}(\bar{\mathbf{u}} - \bar{u}^0\mathbf{e}_r) + \frac{1}{2}a_0 J_{n-1}(\zeta_n)e^{i(n-1)\phi}\mathbf{e}_+ + \frac{1}{2}a_0 J_{n+1}(\zeta_n)e^{i(n+1)\phi}\mathbf{e}_-\right], \\ &= i\omega\Delta\varphi\mathrm{O}F_n\Big\{J_n(\zeta_n)e^{in\phi}(\beta_1 - (1-\beta_1)\cos\theta)\mathbf{e}_z \\ &\quad + \left[\frac{a_0}{2\kappa}J_{n-1}(\zeta_n) - \frac{1}{\sqrt{2}}(1-\beta_1)\sin\theta J_n(\zeta_n)\right]e^{i(n-1)\phi}\mathbf{e}_+ \\ &\quad + \left[\frac{a_0}{2\kappa}J_{n+1}(\zeta_n) - \frac{1}{\sqrt{2}}(1-\beta_1)\sin\theta J_n(\zeta_n)\right]e^{i(n+1)\phi}\mathbf{e}_-\Big\} \\ &= i\omega\Delta\varphi\mathrm{O}F_n\left[JJ^z_n e^{in\phi}\mathbf{e}_z + JJ^+_n e^{i(n-1)\phi}\mathbf{e}_+ + JJ^-_n e^{i(n+1)\phi}\mathbf{e}_-\right], \end{aligned} \tag{A8}$$

where we used $\bar{u}^3 = \kappa\beta_1$ and $\bar{u}^0 = \kappa(1-\beta_1)$ with $\beta_1 = \frac{1}{2}(1 - (1 + a_0^2/2)/(\gamma_0^2(1+\beta_0)^2))$. Equation (A8) for the unchirped case $\alpha = 0$ reduces to the expression found in [25]. Evidently, harmonic n is a superposition of $\ell = n-1$, $\ell = n$, and $\ell = n+1$ orbital angular momentum, each with different polarization and emission amplitude.

[1] L. Allen, M. W. Beijersbergen, R. J. C. Spreeuw, and J. P. Woerdman, Orbital angular momentum of light and the transformation of Laguerre-Gaussian laser modes, Phys. Rev. A **45**, 8185 (1992).

[2] M. F. Andersen, C. Ryu, P. Cladé, V. Natarajan, A. Vaziri, K. Helmerson, and W. D. Phillips, Quantized Rotation of Atoms from Photons with Orbital Angular Momentum, Phys. Rev. Lett. **97**, 170406 (2006).

[3] A. Alexandrescu, D. Cojoc, and E. Di Fabrizio, Mechanism of Angular Momentum Exchange between Molecules and Laguerre-Gaussian Beams, Phys. Rev. Lett. **96**, 243001 (2006).

[4] T. Kuga, Y. Torii, N. Shiokawa, T. Hirano, Y. Shimizu, and H. Sasada, Novel Optical Trap of Atoms with a Doughnut Beam, Phys. Rev. Lett. **78**, 4713 (1997).

[5] M. Padgett and R. Bowman, Tweezers with a twist, Nat. Photon. **5**, 343 (2011).

[6] J. Wang, J. Y. Yang, I. M. Fazal, N. Ahmed, Y. Yan, H. Huang, Y. Ren, Y. Yue, S. Dolinar, M. Tur, and A. E. Willner, Terabit free-space data transmission employing orbital angular momentum multiplexing, Nat. Photon. **6**, 488 (2012).

[7] S. Fürhapter, A. Jesacher, S. Bernet and M. Ritsch-Marte, Spiral interferometry, Opt. Lett. **30**, 1953 (2005).

[8] B. Jack, J. Leach, J. Romero, S. Franke-Arnold, M. Ritsch-Marte, S. M. Barnett, and M. J. Padgett, Holographic Ghost Imaging and the Violation of a Bell Inequality, Phys. Rev. Lett. **103**, 083602 (2009).

[9] J. Leach, B. Jack, J. Romero, A. K. Jha, A. M. Yao, S. Franke-Arnold, D. G. Ireland, R. W. Boyd, S. M. Barnett, and M. J. Padgett, Quantum correlations in optical angle-orbital angular momentum variables, Science **329**, 662 (2010).

[10] M. Malik, M. Erhard, M. Huber, M. Krenn, R. Fickler, and A. Zeilinger, Multi-photon entanglement in high dimensions, Nat. Photon. **10**, 248 (2016).

[11] M. van Veenendaal and I. McNulty, Prediction of Strong Dichroism Induced by X Rays Carrying Orbital Momentum, Phys. Rev. Lett. **98**, 157401 (2007).

[12] C. Stamm, N. Pontius, T. Kachel, M. Wietstruk, and H. A. Dürr, Femtosecond x-ray absorption spectroscopy of spin and orbital angular momentum in photoexcited Ni films during ultrafast demagnetization, Phys. Rev. B **81**, 104425 (2010).

[13] A. Picón, J. Mompart, J. R. Vázquez de Aldana, L. Plaja, G. F. Calvo, L. Roso, L. Allen, M. V. Beijersbergen, R. J. C Spreeuw, and J. P. Woerdman, Photoionization with orbital angular momentum beams, Opt. Express **18**, 3660 (2010).

[14] M. Hentschel, R. Kienberger, C. Spielmann, G. A. Reider, N. Milosevic, T. Brabec, P. Corkum, U. Heinzmann, M. Drescher, and F. Krausz, Attosecond metrology, Nature (London) **414**, 509 (2001).

[15] A. P. Mancuso, A. G. Peele, B. Lai, C. Q. Tran, D. Paterson, E. Harvey, I. McNulty, J. P. Hayes, K. A. Nugent, and P. J. McMahon, Observation of an x-ray vortex, Opt. Lett. **27**, 1752 (2002).

[16] K. Sueda, G. Miyaji, N. Miyanaga, M. Nakatsuka, L. Allen, M. W. Beijersbergen, R. J. C Spreeuw, and J. P. Woerdman, Laguerre-Gaussian beam generated with a multilevel spiral phase plate for high intensity laser pulses, Opt. Express **12**, 3548 (2004).

[17] M. Zürch, C. Kern, P. Hansinger, A. Dreischuh, and C. Spielmann, Strong-field physics with singular light beams, Nat. Phys. **8**, 743 (2012).

[18] C. Hernández-García, A. Picón, J. San Román, and L. Plaja, Attosecond Extreme Ultraviolet Vortices from High-Order Harmonic Generation, Phys. Rev. Lett. **111**, 083602 (2013).

[19] G. Gariepy, J. Leach, K. T. Kim, T. J. Hammond, E. Frumker, R. W. Boyd, and P. B. Corkum, Creating High-Harmonic Beams with Controlled Orbital Angular Momentum, Phys. Rev. Lett. **113**, 153901 (2014).

[20] A. D. Shiner, C. Trallero-Herrero, N. Kajumba, H. C. Bandulet, D. Comtois, F. Légaré, M. Giguère, J. C. Kieffer, P. B. Corkum, and D. M. Villeneuve, Wavelength Scaling of High Harmonic Generation Efficiency, Phys. Rev. Lett. **103**, 073902 (2009).

[21] G. Sansone, L. Poletto, and M. Nisoli, High-energy attosecond light sources, Nat. Photon. **5**, 655 (2011).

[22] J. Bahrdt, K. Holldack, P. Kuske, R. Müller, M. Scheer, and P. Schmid, First Observation of Photons Carrying Orbital Angular Momentum in Undulator Radiation, Phys. Rev. Lett. **111**, 034801 (2013).

[23] E. Hemsing, A. Knyazik, M. Dunning, D. Xiang, A. Marinelli, C. Hast, and J. B. Rosenzweig, Coherent optical vortices from relativistic electron beams, Nat. Phys. **9**, 549 (2013).

[24] P. R. Ribič, B. Rösner, D. Gauthier, E. Allaria, F. Döring, L. Foglia, L. Giannessi, N. Mahne, M. Manfredda, C. Masciovecchio, R. Mincigrucci, N. Mirian, E. Principi, E. Roussel, A. Simoncig, S. Spampinati, C. David, and G. De Ninno, Extreme-Ultraviolet Vortices from a Free-Electron Laser, Phys. Rev. X **7**, 031036 (2017).

[25] Y. Taira, T. Hayakawa, and M. Katoh, Gamma-ray vortices from nonlinear inverse Thomson scattering of circularly polarized light, Sci. Rep. **7**, 5018 (2017).

[26] E. Esarey, S. K. Ride, and P. Sprangle, Nonlinear Thomson scattering of intense laser pulses from beams and plasmas, Phys. Rev. E **48**, 3003 (1993).

[27] B. H. Schaap, P. W. Smorenburg, and O. J. Luiten, Isolated attosecond x-ray pulses from superradiant thomson scattering by a relativistic chirped electron mirror, Sci. Rep. **12**, 19727 (2022).

[28] J. D. Jackson, Classical electrodynamics, 3rd ed. (1998).

[29] V. Petrillo, A. Bacci, C. Curatolo, I. Drebot, A. Giribono, C. Maroli, A. R. Rossi, L. Serafini, P. Tomassini, C. Vaccarezza, and A. Variola, Polarization of x-gamma radiation produced by a Thomson and Compton inverse scattering, Phys. Rev. ST Accel. Beams **18**, 110701 (2015).

[30] W. S. Graves, F. X. Kärtner, D. E. Moncton, and P. Piot, Intense Superradiant X Rays from a Compact Source Using a Nanocathode Array and Emittance Exchange, Phys. Rev. Lett. **108**, 263904 (2012).

[31] B. H. Schaap, T. D. C. de Vos, P. W. Smorenburg, and O. J. Luiten, Photon yield of superradiant inverse Compton scattering from microbunched electrons, New J. Phys. **24**, 033040 (2022).

[32] J. Duris, S. Li, T. Driver, E. G. Champenois, J. P. MacArthur, A. A. Lutman, Z. Zhang, P. Rosenberger, J. W. Aldrich, R. Coffee, G. Coslovich, F. J. Decker, J. M. Glownia, G. Hartmann, W. Helml, A. Kamalov, J. Knurr, J. Krzywinski, M. F. Lin, J. P. Marangos *et al.*, Tunable isolated attosecond x-ray pulses with gigawatt peak power from a free-electron laser, Nat. Photon. **14**, 30 (2020).

[33] T. Tanaka, Proposal to Generate an Isolated Monocycle X-Ray Pulse by Counteracting the Slippage Effect in Free-Electron Lasers, Phys. Rev. Lett. **114**, 044801 (2015).

[34] D. Gauthier, P. R. Ribic, G. Adhikary, A. Camper, C. Chappuis, R. Cucini, L. F. Dimauro, G. Dovillaire, F. Frassetto, R. Géneaux, P. Miotti, L. Poletto, B. Ressel, C. Spezzani, M. Stupar, T. Ruchon, and G. De Ninno, Tunable orbital angular momentum in high-harmonic generation, Nat. Commun. **8**, 14971 (2017).

[35] M. Kozák, T. Eckstein, N. Schönenberger, and P. Hommelhoff, Inelastic ponderomotive scattering of electrons at a high-intensity optical travelling wave in vacuum, Nat. Phys. **14**, 121 (2018).

[36] B. H. Schaap, C. W. Sweers, P. W. Smorenburg, and O. J. Luiten, Ponderomotive bunching of a relativistic electron beam for a superradiant Thomson source, Phys. Rev. Accel. Beams **26**, 074401 (2023).

[37] N. Schönenberger, A. Mittelbach, P. Yousefi, J. McNeur, U. Niedermayer, and P. Hommelhoff, Generation and Characterization of Attosecond Microbunched Electron Pulse Trains via Dielectric Laser Acceleration, Phys. Rev. Lett. **123**, 264803 (2019).